

# Superconductivity in the tungsten bronze $\text{Rb}_x\text{WO}_3$ ( $0.20 \leq x \leq 0.33$ ) in connection with its structure, electronic density of states, and phonon density of states

R. Brusetti,\* P. Bordet, and J. Bossy

*Institut NEEL, CNRS and UJF, Boîte Postale 166, 38042 Grenoble Cedex 9, France*

H. Schober and S. Eibl

*Institut Laue Langevin, Boîte Postale 156, 38042 Grenoble Cedex 9, France*

(Received 4 April 2007; revised manuscript received 6 September 2007; published 15 November 2007)

We have measured the magnetic susceptibility of the  $\text{Rb}_x\text{WO}_3$  compound ( $0.20 \leq x \leq 0.33$ ) and examined its structural properties and lattice dynamics, using elastic and inelastic neutron scattering (INS) experiments, in order to gain further insight into the unusual features of its superconducting state, namely, (i) the stabilizing effect resulting from the reduction of rubidium content, i.e., of the conduction electron density [what we shall name the “ $T_c(x)$  paradox”], and (ii) the destabilizing effect of the ordering of the Rb ions. We also performed density-functional calculations of the phonon dispersion in the “stoichiometric”  $\text{Rb}_{0.33}\text{WO}_3$  and  $\text{Cs}_{0.33}\text{WO}_3$  to identify the main features of the phonon spectra. These calculations give a very satisfactory description of the INS data and confirm the assignment to these bronzes of a lower (orthorhombic) symmetry than previously proposed. Our results contradict the previous interpretations of the  $T_c(x)$  paradox and of the ordering effect: (i) no general softening of the lattice accompanies the increase of the Rb-vacancy population and (ii) no general decrease of the electron density of states  $D_{\text{EF}}$  distinguishes the ordered nonsuperconducting  $\text{Rb}_{0.25}\text{WO}_3$  from its neighboring disordered parents. It appears, therefore, that the electron-electron coupling in this system probably proceeds through well-defined electronic states and phonons. This is a feature these “hexagonal” tungsten bronzes (HTB) apparently share with several high- $T_c$  materials. We discuss what could be the mechanisms responsible for the very selective electron-phonon coupling in the HTB.

DOI: [10.1103/PhysRevB.76.174511](https://doi.org/10.1103/PhysRevB.76.174511)

PACS number(s): 74.62.-c, 61.12.-q, 74.25.Kc, 71.15.Mb

## I. INTRODUCTION

The transport properties of the tungsten bronzes of general formula  $M_x\text{WO}_3$  ( $M$ =alkali atoms) and, particularly, the ability of some of these oxides—those having the “tetragonal I” or hexagonal symmetry<sup>1</sup>—to form superconducting ground states have given rise to large numbers of investigations and interpretations for more than 40 years. In this system, like in many others, a lot of confusion has been introduced by contradictory results, to be principally attributed to inadequate characterization of the samples. Now that this point has been improved, it is possible to see more clearly what features the tungsten bronzes share with other superconductors—often much more documented because of their higher transition temperature  $T_c$ —and, on the contrary, to what extent they pose a specific problem. First, it seems clear that a parallel can be drawn with the barium bismuthate system because both systems are built from a parent insulating oxide— $\text{WO}_3$  and  $\text{BaBiO}_3$ , respectively—via a kind of heavy doping (which, in the case of the bronzes, is somewhat reminiscent of an intercalation process). In both systems, the doping range where a metallic but highly resistive behavior is observed is rather narrow and corresponds to a structure with a higher symmetry than the neighboring phases. In this narrow range,  $T_c$  strongly depends on the doping level, and is the highest at the lowest level compatible with the stability of the phase. Another feature these two systems have in common is the type of building blocks that make up the lattice, i.e., the corner-bound  $\text{WO}_6$  and  $\text{BaBiO}_6$  octahedra, which can connect together in many ways, but can also accommodate various kinds of distortions, in connection with the elec-

tron population. It is, therefore, not surprising to observe polaronic effects in the nonmetallic phases. Since up to now no traces of magnetism have been found in these oxides, in which the electronic density of states is quite low, it is generally concluded that very special electron-lattice interactions are involved in the stabilization of the superconducting ground state. In the case of  $\text{Ba}_{1-x}\text{K}_x\text{BiO}_3$  (BKBO), which has given rise to the most extensive studies (maximum  $T_c \approx 35$  K), it seems that this robust stabilization can be accounted for—in the framework of the Eliashberg strong-coupling theory—by the particular strength of the electron coupling with high-energy oxygen phonons, probably those corresponding to bond-stretching modes. However, it has still not been established which among these modes are the more effective within the 30–70 meV energy range.<sup>2–4</sup> Considering now the  $M_x\text{WO}_3$  system and, more precisely, the superconducting tetragonal I and “hexagonal” phases, we distinguish first—leaving apart the lower  $T_c$ —the specific role of stoichiometry: in these compounds, doping is achieved by intercalating the  $M$  atoms in some cages or tunnels available between a skeleton of  $\text{WO}_6$  octahedra. Only in the hexagonal tungsten bronzes (HTBs) can one speak about a “stoichiometric” composition  $M_{0.33}\text{WO}_3$ , for which all the (tunnel) sites are occupied by alkali atoms of appropriate size (K, Rb, and Cs). Reducing the doping creates vacancies on these sites and opens up the possibility of disorder. This vacancy disorder differs in its nature from the substitutional disorder in the BKBO system, where barium is partially replaced by potassium. Both have in common that order can be established rather easily. In  $\text{K}_x\text{WO}_3$  and  $\text{Rb}_x\text{WO}_3$ , this happens near room temperature or slightly below, respectively.

The effect on  $T_c$  of ordering among the doping population in BKBO<sup>5</sup> has still not been studied. In the high- $T_c$  cuprates (YBaCuO), it sensibly increases  $T_c$ .<sup>6</sup> Ordering of the vacancies in the rubidium and potassium HTBs drastically destabilizes superconductivity.<sup>8</sup> In principle, this provides the opportunity of identifying the signature(s) of electron-phonon coupling by comparing the relevant properties (structure, electronic density of states, and phonon density of states) in superconducting disordered and in nonsuperconducting ordered  $M_x\text{WO}_3$ . Actually, no such straightforward comparison is possible in the BKBO system, for instance, because the nonsuperconducting parents have very different structures and electron populations. On the contrary, in the HTB, superconductivity can settle or not in two very similar landscapes. We have focused our investigations on the rubidium HTB (maximum  $T_c \approx 5.5$  K), which is the most suited for the comparison we had in mind as it stands just between  $\text{K}_x\text{WO}_3$ —in which the ordering does not leave much place for superconductivity—and  $\text{Cs}_x\text{WO}_3$ , in which no ordering occurs. After a short description of the experimental techniques we have used in this study, we shall present below (i) the results of our magnetic susceptibility measurements, from which we can judge the relevance of the electronic density of states to the stability of the superconducting state; (ii) the structural information obtained from our elastic neutron diffraction experiments, complementing the previous x-ray study on a single crystal;<sup>7</sup> and (iii) finally, the generalized phonon density of states we have deduced from our inelastic neutron scattering (INS) experiments. These data will be compared to the results of our density-functional calculations. A general discussion will follow, in which we consider the pieces of information provided by our study and how they orientate further investigations.

## II. EXPERIMENT AND CALCULATION

### A. Samples

All the measurements we are to report have been made on microcrystallized samples which had been prepared by the usual solid-state reaction of high purity W,  $\text{WO}_3$ , and  $\text{Rb}_2\text{WO}_4$  in sealed quartz tubes as described in Ref. 8. We focused our attention on three  $\text{Rb}_x\text{WO}_3$  compounds with quite different behaviors as far as superconductivity is concerned. The first compound is the stoichiometric one ( $x=0.33$ ), in which all the tunnel sites are occupied, its  $T_c$  is about 2.2 K; the second one has 1/4 of the tunnel sites vacant ( $x=0.25$ ), these vacancies are ordered below about 240 K and the superconducting state only appears below about 0.2 K. The third compound has a vacancy content (about 40%) which places it very close to the boundary of the HTB phase, where  $T_c$  is the highest (about 5 K) and where the destabilizing effect of the vacancy ordering can be easily shown. Its nominal rubidium content corresponds to  $x=0.20$  (Ref. 9); however, the x-ray scattering spectrum of this preparation reveals that it contains approximately 5% of the intergrowth tungsten bronze (ITB), whose formula is probably  $\text{Rb}_{0.10}\text{WO}_3$ .<sup>10</sup> Therefore, the majority HTB phase is likely to have a Rb content corresponding to  $x=0.205$ .<sup>11</sup> As will be discussed later, this small amount of ITB in the  $x$

$=0.20$  preparation cannot significantly affect its magnetic properties; it should have no influence either on the generalized phonon density of state  $G(\omega)$  deduced from the inelastic neutron scattering experiments. However, it will not allow us to carry out any crystal structure refinement from the elastic neutron scattering experiments performed on this sample.

### B. Magnetic susceptibility

We performed magnetic susceptibility measurements with a MPMS XL Quantum Design superconducting quantum interference device magnetometer. In this kind of apparatus, the sample is positioned between the detection coils by fixing it on a straw. As the magnetic moments, which we had to measure, were quite weak, we choose to minimize the sample holder contribution by preparing composite samples in the following way: the crystallized powder was mixed with epoxy and molded to obtain a cylinder which could be maintained within the straw by friction only. As this straw is much longer than the distance between the detection coils, it should give no signal, provided it is perfectly homogeneous. However, even by using always the same straw, we did not achieve a reproducibility of our measurements better than about 2%. This could be due to the imperfect homogeneity of the straw or/and to the fact that the lateral centering of the sample cannot be guaranteed with sufficient accuracy. Since the susceptibility of the epoxy (Vishay 610 in this case) is more than an order of magnitude larger (about  $-5.5 \times 10^{-7}$  uem/g) than the susceptibility  $\chi_x$  of the bronzes, we reduced its content in the composite samples to the minimum (about 5% of the total mass). The resulting absolute accuracy of our determination of  $\chi_x$  is estimated at about  $10^{-9}$  uem/g, whereas the sensitivity of the measurements is better than  $10^{-10}$  uem/g. In order to check the isotropy of the magnetic properties, we also prepared oriented samples by mixing the bronze powder with a special epoxy, introducing the mixture (60:40 mass ratio) into a 15 T magnetic field and hardening the mixture by raising its temperature to 120 °C for 6 min. The orientation of the  $\text{Rb}_x\text{WO}_3$  microcrystals with their  $c$  axis parallel to the applied field is clearly observed under a microscope and confirmed by an x-ray observation, which indicates that the susceptibility is larger along this direction.<sup>12</sup> However, this method of orienting the powders did not give us quantitative results as we were unable to estimate the epoxy content in the samples and, therefore, the epoxy contribution to  $\chi$ —which now largely overcomes that of  $\text{Rb}_x\text{WO}_3$ —with sufficient accuracy. Moreover, this process has the potential of introducing some parasitic magnetic moments, as was observed in some high- $T_c$  cuprates.<sup>13</sup>

### C. Elastic neutron scattering experiments

These experiments were performed on the high-resolution neutron powder diffractometer D2B of the ILL, Grenoble, France. The samples were placed in a 10 mm diameter cylindrical vanadium can inside a closed-cycle pulse-tube cryostat. Diffractograms were recorded between  $2\theta=0^\circ$  and  $160^\circ$  at a constant step of  $0.05^\circ$ , at different temperatures between 5 and 300 K, using the  $\lambda=1.594$  Å wavelength obtained from the (335) reflection of the Ge monochromator. In

order to improve the spatial resolution, we also collected two diffractograms with  $\lambda=2.4$  Å at  $T=5$  K for the  $x=0.25$  and 0.20 samples, for which additional superstructure reflections due to ordering of the Rb cations were expected. All refinements were carried out using the WINPLOTR software suite.<sup>14</sup>

#### D. Inelastic neutron scattering experiments

The INS measurements were performed on the cold neutron time-of-flight spectrometer IN6 of the ILL. The incident wavelength was 4.12 Å, and neutrons were detected over the scattering angles from 13° to 114°. We used a slightly inelastic focusing ( $E_{\text{focus}}=2.7$  meV) to improve resolution at large energy transfers in upscattering (neutron energy gain mode). The raw data were corrected for empty container scattering and normalized to a vanadium standard. The spectra thus obtained were converted into generalized phonon density of states (GDOS)  $G(\omega)$  using the incoherent approximation. Multiphonon corrections were performed self-consistently. The neutron-weighted GDOS is related to the true partial phonon density of states  $g_i(\omega)$  ( $i=\text{Rb, W, and O}$ ) according to

$$G(\omega) = \frac{\sum_{i=\text{Rb,W,O}} (c_i \sigma_i / m_i) g_i(\omega)}{\sum_{i=\text{Rb,W,O}} (c_i \sigma_i / m_i)},$$

where  $c_i$  indicates the concentration,  $\sigma_i$  the total bound scattering cross section for atoms  $i$ , and  $m_i$  is its mass. Consequently,  $G(\omega)$  is related to the true total phonon density of states  $g(\omega)$  by a frequency-dependent factor  $f(\omega) = g(\omega)/G(\omega)$  which has no simple expression here as the  $\sigma_i/m_i$  are very different.

#### E. Density-functional calculations

We have calculated the phonon dispersion relations and phonon density of states of the stoichiometric compounds  $\text{Rb}_{0.33}\text{WO}_3$  and  $\text{Cs}_{0.33}\text{WO}_3$  using the software PHONON.<sup>15</sup> PHONON uses the direct method to set up a dynamical matrix from Hellmann-Feynman forces. In our case, the Hellmann-Feynman forces were provided by *ab initio* calculations performed within the density-functional theory (DFT), using the projector augmented wave potentials<sup>16,17</sup> and the generalized gradient approximation, as implemented in the VASP software.<sup>18,19</sup> We choose  $2s^2 1p^4$ ,  $4p^6 5s^1$ ,  $5s^2 5p^6 6s^1$ , and  $5d^4 6s^2$  valence electron configurations for O, Rb, Cs, and W, respectively. The maximum energy cutoff was 283 eV.

The Hellmann-Feynman forces are calculated with respect to a completely relaxed structure with no residual forces acting on the various atoms ( $F_{\text{residual}} \leq 0.005$  eV/Å,  $1$  eV/Å = 0.016 02 nN). In the first stage of the relaxation process, we optimized the structural parameters of the primitive cell. In a second step, the supercell parameters were obtained using a  $\mathbf{k}: 1 \times 1 \times 1$  mesh for the wave vector summation over electronic states. The optimized theoretical structure was then used to determine the Hellmann-Feynman forces for symmetry independent displacement with the amplitude of 0.05 Å.

The use of a rather extended supercell containing more than 200 atoms is mandatory as the force constants fall off rather slowly with distance. All phonon calculations on single cells predict, therefore, unstable crystals, i.e., their dynamical matrix  $D(\vec{q})$  for some  $\vec{q}$  possesses negative eigenvalues, leading, in theory, to relaxational modes. The  $\text{Rb}_{0.33}\text{WO}_3$  calculations in the  $C222_1$  symmetry group were, e.g., carried out on a supercell containing 208 atoms with a dimension of roughly  $12.9 \times 14.9 \times 15.3$  Å<sup>3</sup>. We also calculated the neutron-weighted phonon density of states (DOS)  $G(\omega)$  and the weighting factor  $f(\omega)$ .

### III. RESULTS

#### A. Magnetic properties

We can summarize the main results of these measurements as follows:

(i) At low field, the magnetic susceptibility of our samples is field dependent, even at room temperature, showing a paramagnetic contribution  $\chi_p$  saturating below 1 T; this contribution is noticeably larger in the oriented samples and probably results from a pollution by ferromagnetic particles—representing less than  $10^{-6}$  of the sample mass in the case of Fe particles. This contribution has been removed in the data presented below.

(ii) The temperature dependence of  $\chi$  is only sensible below 100 K, where it resembles the contribution of magnetic impurities.<sup>20</sup> We fitted the low-temperature behavior ( $T \leq 120$  K) with a Curie-Weiss term  $\frac{C}{T-\theta}$  and found that it could correspond to about 30–50 ppm of  $\text{Fe}^{3+}$ . These impurities are probably coming mostly from the  $\text{Rb}_2\text{WO}_4$  starting powder; however, the  $C$  values derived from this fit are not clearly correlated with the Rb content,  $x$ .<sup>21</sup> The characteristic temperature  $\theta$  seems to increase with  $x$ , between  $0 \pm 0.5$  K and  $6.8 \pm 1.5$  K.<sup>22</sup> By removing these Curie-Weiss terms from our data, we obtain the “intrinsic” susceptibilities  $\chi_x$  plotted in Fig. 1.

(iii) The order-disorder (OD) transition of the rubidium atoms is clearly seen in  $\text{Rb}_{0.25}\text{WO}_3$  at  $T_{\text{OD}} \approx 250$  K. It has been also observed at about 220 K in another experiment, on a sample (sample 2) coming from another batch (see inset in Fig. 1). It has been shown previously<sup>8</sup> that the order-disorder transition becomes more and more continuous as the rubidium content deviates from  $x=0.25$ , which explains why it cannot be observed in  $\text{Rb}_{0.20}\text{WO}_3$ . It should also be mentioned that the order-disorder anomaly occurs at a lower temperature in sample 2. This shift of  $T_{\text{OD}}$  comes from slightly different  $x$  and, incidentally, confirms the rapid lowering of  $T_{\text{OD}}$  with the departure from the optimal  $x=0.25$  rubidium content. The larger ordering-induced susceptibility increase in sample 2, however, cannot be explained in the same way. It is more probably related to the use of a lower field (1 T), and this is born out by the still higher anomaly observed in the same sample with a 0.1 T field.

(iv) As displayed in Fig. 2, the magnetic susceptibility does not depend significantly on the Rb content, which confirms the previous data of Wanlass and Sienko.<sup>23</sup> Our data, however, are about  $10^{-8}$  emu/g above those of Wanlass and

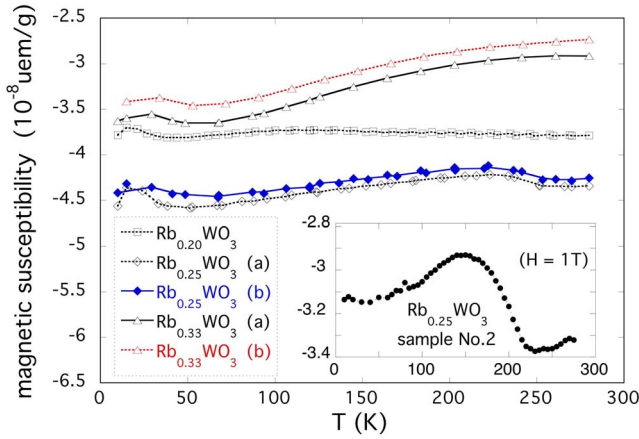


FIG. 1. (Color online) Magnetic susceptibility of the  $\text{Rb}_x\text{WO}_3$  powder samples as a function of temperature. The difference between the data obtained on two samples (a) and (b) of the same batch, for  $x=0.25$  and  $0.33$ , gives an estimate of their absolute accuracy. The impurity contributions have been subtracted (see text). The inset corresponds to a measurement on a sample from another batch, with another magnetometer and a different sample holder, for which the *absolute* accuracy cannot be guaranteed. Lines are only guides for the eye.

Sienko, on average, i.e., well beyond the estimated accuracy of both results.<sup>24</sup> Such a discrepancy is quite common when low-susceptibility samples of different origins, measured with different techniques, are compared. It probably indicates that some random errors have been overlooked. This is illustrated, for instance, by the case of  $\text{WO}_3$  we shall have to refer to below.

### B. Structural properties

In a previous work,<sup>7</sup> we have examined the structure of the stoichiometric  $\text{Rb}_{0.33}\text{WO}_3$  compound using x-ray single crystal diffraction. The observation of unexpected  $(h0l)$ ,  $l$

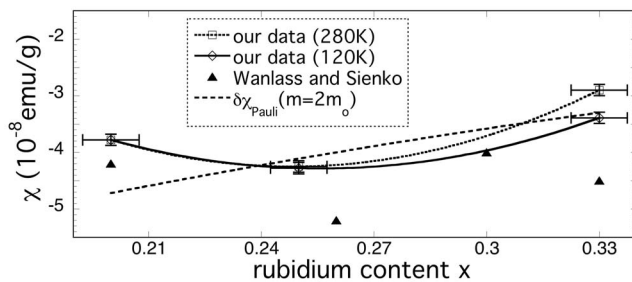


FIG. 2. Magnetic susceptibility of the  $\text{Rb}_x\text{WO}_3$  powder samples at 280 K (dotted line) and 120 K (solid line) as a function of the rubidium content  $x$ . The previous data of Wanlass and Sienko (Ref. 23) have been included ( $\blacktriangle$ ). The dashed line represents what would be the  $x$  dependence of a Pauli contribution  $\chi_{spin}$  in a quasi-free-electron model with an effective mass two times the electron mass  $m_0$  (a diamagnetic contribution has been added to  $\chi_{spin}$  in order to obtain  $\chi_x \approx -3.3 \times 10^{-8}$  emu/g for  $x=0.33$ ). Other lines are guides for the eye.

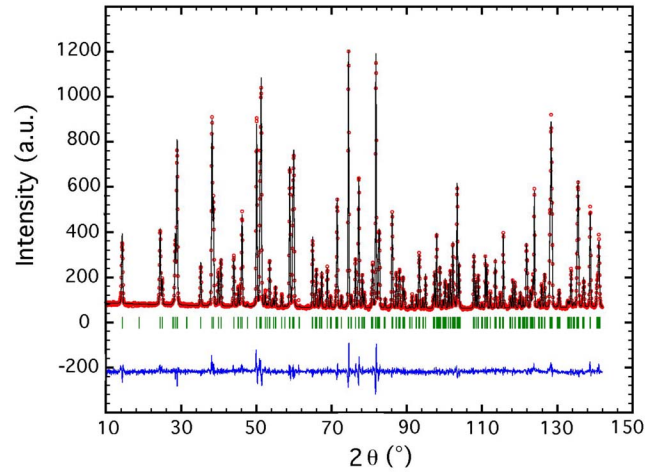


FIG. 3. (Color online) Observed neutron diffraction pattern along with calculated and difference patterns from the Rietveld refinement of  $\text{Rb}_{0.33}\text{WO}_3$  at 5 K.

$=2n+1$ , reflections for the reported  $P6_3/mcm$  space group had lead us to search for a lower symmetry. Two solutions yielding structure refinements with reasonable agreement factors were proposed with the  $P6_3$  and  $P3$  space groups. The presence of at least a threefold axis along  $c$  was supported by the absence of a detectable unit cell distortion or twinning. The neutron diffraction experiments we are to present were meant to complement these investigations. The first attempts to perform a full pattern matching of the  $x=0.33$  data at  $T=5$  K rapidly demonstrated that they could not be fitted using a hexagonal unit cell. This was evidenced by large discrepancies in the reflection positions, indicating a unit cell distortion. A  $\chi^2$  agreement factor of 10.8 was obtained for a pattern matching refinement with the  $P3$  space group. The data could be successfully fitted by using monoclinic symmetry, yielding a  $\chi^2$  of 2.2 for a pattern matching refinement with the  $P2_1$  space group. The structure was then

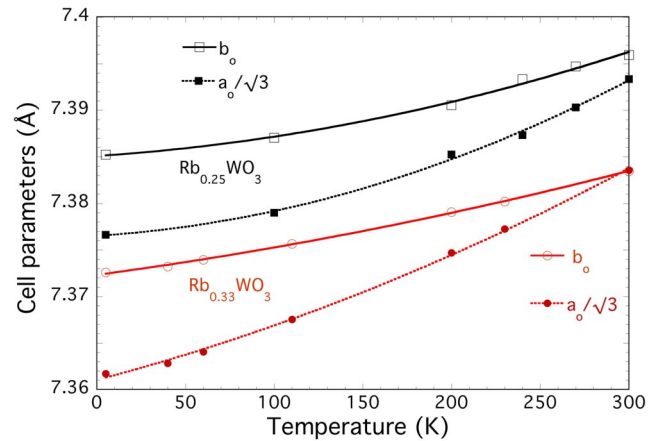


FIG. 4. (Color online) Temperature dependence of the  $C222_1$  cell parameters in  $\text{Rb}_{0.25}\text{WO}_3$  (squares) and  $\text{Rb}_{0.33}\text{WO}_3$  (circles); empty symbols and solid lines correspond to  $b_0=b$ , full symbols and dotted lines correspond to  $a_0/\sqrt{3}$ . Lines are second-order polynomial fits.

TABLE I. Structural parameters refined for  $\text{Rb}_x\text{WO}_3$  with space group  $C222_1$  at 5 and 300 K. In each row, the upper data correspond to  $\text{Rb}_{0.33}\text{WO}_3$  and the lower data to  $\text{Rb}_{0.25}\text{WO}_3$ .

Atom	Pos.	<i>x</i>		<i>y</i>		<i>z</i>	
		<i>T</i> =5 K	<i>T</i> =300 K	<i>T</i> =5 K	<i>T</i> =300 K	<i>T</i> =5 K	<i>T</i> =300 K
W1	4	0.0000	0.0000	0.4794(7) 0.4768(2)	0.481(2) 0.472(2)	0.0000	0.0000
W2	8	0.7596(3) 0.7583(9)	0.758(1) 0.759(1)	0.7580(8) 0.759(2)	0.759(3) 0.758(2)	0.2473(6) 0.254(1)	0.2492(8) 0.251(1)
Rb	4	0.0097(2) 0.0015(9)	0.0065(5) 0.0022(8)	0.0000	0.0000	0.0000	0.0000
O1	8	0.6065(3) 0.6071(8)	0.607(1) 0.6084(7)	0.8138(7) 0.816(1)	0.815(2) 0.816(1)	0.270(1) 0.266(2)	0.2571(8) 0.262(1)
O2	8	0.7883(2) 0.7895(5)	0.7919(5) 0.7907(5)	0.0039(8) 0.004(2)	0.004(3) 0.004(2)	0.2233(4) 0.223(1)	0.2230(7) 0.2317(7)
O3	8	0.6031(3) 0.6031(8)	0.6055(9) 0.6044(7)	0.1845(7) 0.182(1)	0.181(2) 0.182(1)	0.273(1) 0.269(2)	0.2696(9) 0.269(1)
O4	4	0.5178(2) 0.5171(5)	0.5094(7) 0.5132(4)	0.0000	0.0000	0.0000	0.0000
O5	8	0.2333(1) 0.2353(3)	0.2400(3) 0.2385(3)	0.2286(3) 0.2283(8)	0.230(1) 0.2335(9)	0.0000(6) 0.0079(9)	-0.0007(9) 0.0030(8)

solved and refined in  $P2_1$  symmetry, with agreement factors  $R_p=9.70\%$ ,  $R_{wp}=10.3\%$ , and  $\chi^2=3.69$ , and the unit cell parameters:  $a=7.372\ 63(6)\ \text{\AA}$ ,  $b=7.530\ 91(4)\ \text{\AA}$ ,  $c=7.3650(2)\ \text{\AA}$ , and  $\beta=120.043(2)^\circ$ . The Rietveld fit to our neutron diffraction data at 5 K is shown in Fig. 3.

Similar refinements were then carried out for all temperatures up to 300 K. The corresponding Rietveld fits are given in Ref. 25. One observes that the very small difference between  $a$  and  $c$ , and the deviation of  $\beta$  from  $120^\circ$  gradually decrease on heating and vanish at room temperature. This explains why the distortion could not be detected by single crystal x-ray diffraction at room temperature. It is also worth noting that the structure description in  $P2_1$  symmetry requires 13 independent atoms (3 tungsten 1 rubidium, and 9 oxygen atoms), all on a general position, resulting in 38 positional parameters (the  $y$  parameter of Rb was kept equal to 0 in order to fix the origin along the  $b$  axis). This leads to strong correlations between parameters in this pseudosymmetric structure description and makes it difficult to obtain a proper convergence of the refinements, especially close to room temperature where the distortion vanishes. Therefore, we searched for solutions with a higher symmetry and which would provide more stable refinements. We found that a satisfactory fit to the 5 K data could be found by using the C-centered orthorhombic unit cell with

$$\vec{a}_o = \vec{a} + 2\vec{b}, \quad \vec{b}_o = -\vec{a}, \quad \vec{c}_o = \vec{c},$$

leading to  $a_o = a\sqrt{3}$ ,  $b_o = b$ , and  $c_o = c$ . The volume of this cell is twice that of the original hexagonal cell (and of the mono-

clinic cell given above). The best result for the Rietveld refinement of the structure was obtained with space group  $C222_1$  ( $\chi^2=2.6$ ), for which only 8 independent atoms (2 tungsten, 1 rubidium, and 5 oxygen atoms) and 18 positional parameters are required. Similar refinements were carried out on the diffractograms obtained at higher temperatures without noticing any deterioration of the convergence up to 300 K, which confirms that this model does not induce excessive correlations between positional parameters. Here,

TABLE II. Agreement factors, cell parameters, and atomic displacement parameters of  $\text{Rb}_{0.33}\text{WO}_3$  and  $\text{Rb}_{0.25}\text{WO}_3$  at  $T=5$  and 300 K.

	$\text{Rb}_{0.33}\text{WO}_3$		$\text{Rb}_{0.25}\text{WO}_3$	
	<i>T</i> =5 K	<i>T</i> =300 K	<i>T</i> =5 K	<i>T</i> =300 K
$R_p$ (%)	9.79	12.2	17.2	11.6
$R_{wp}$ (%)	10.4	11.9	17.8	11.7
$\chi^2$	3.71	3.78	6.43	4.01
$R_{\text{Bragg}}$ (%)	4.15	5.29	9.58	5.74
$a$ ( $\text{\AA}$ )	12.7509(1)	12.7887(2)	12.7766(4)	12.8056(4)
$b$ ( $\text{\AA}$ )	7.37259(6)	7.3835(2)	7.3853(2)	7.3959(2)
$c$ ( $\text{\AA}$ )	7.53086(5)	7.56749(6)	7.5037(1)	7.53745(8)
$B_O$ ( $\text{\AA}^2$ )	0.488(13)	0.83(2)	0.76(3)	0.88(2)
$B_{\text{Rb}}$ ( $\text{\AA}^2$ )	0.93(3)	3.51(6)	3.4(1)	4.60(8)
$B_W$ ( $\text{\AA}^2$ )	0.33(2)	0.60(2)	0.2(3)	0.71(3)

TABLE III. Cation-anion distances for  $\text{Rb}_{0.33}\text{WO}_3$  and  $\text{Rb}_{0.25}\text{WO}_3$  at  $T=5$  and 300 K from the Rietveld refinement results given in Tables I and II. Distortion is defined as  $\sum_{i=1}^n (d_i - \bar{d})^2 / n\bar{d}^2$ , where  $n$  is the number of nearest neighbors (14 for Rb). BVS are bond valence sums calculated according to Ref. 26.

Atoms	$\text{Rb}_{0.33}\text{WO}_3$		$\text{Rb}_{0.25}\text{WO}_3$	
	$T=5$ K	$T=300$ K	$T=5$ K	$T=300$ K
W1-O1 ( $\times 2$ )	1.832(6)	1.84(2)	1.81(1)	1.81(1)
W1-O3 ( $\times 2$ )	2.011(6)	2.00(2)	2.01(1)	2.05(1)
W1-O4 ( $\times 2$ )	1.9024(5)	1.901(1)	1.896(1)	1.903(1)
Average	1.915(2)	1.917(1)	1.907(5)	1.921(5)
Distortion ( $\times 10^4$ )	14.70	12.66	18.40	25.60
BVS		6.1(1)	6.30(8)	6.15(8)
W2-O1	2.002(6)	1.97(3)	1.98(2)	1.98(2)
W2-O2	1.858(8)	1.86(3)	1.87(2)	1.87(2)
W2-O2	1.983(8)	2.00(3)	1.99(2)	1.99(2)
W2-O3	1.839(6)	1.84(2)	1.87(2)	1.84(1)
W2-O5	1.908(6)	1.895(9)	1.91(1)	1.90(1)
W2-O5	1.905(6)	1.92(1)	1.88(1)	1.90(1)
Average	1.916(3)	1.913(9)	1.916(6)	1.913(6)
Distortion ( $\times 10^4$ )	9.73	8.12	6.82	7.72
BVS		6.1(1)		6.1(1)
Rb1-O1 ( $\times 2$ )	3.319(8)	3.30(1)	3.36(1)	3.35(1)
Rb1-O1 ( $\times 2$ )	3.247(7)	3.30(1)	3.23(1)	3.27(1)
Rb1-O2 ( $\times 2$ )	3.286(3)	3.262(8)	3.18(1)	3.22(1)
Rb1-O2 ( $\times 2$ )	3.313(3)	3.276(8)	3.38(1)	3.33(1)
Rb1-O3 ( $\times 2$ )	3.324(8)	3.36(1)	3.36(1)	3.37(1)
Rb1-O3 ( $\times 2$ )	3.312(3)	3.434(8)	3.43(1)	3.48(1)
Average	3.290(2)	3.313(3)	3.309(3)	3.326(3)
Distortion ( $\times 10^4$ )	1.17	3.15	7.41	4.99
BVS		0.829(7)		0.820(8)

again, the very small structural distortion [which can be represented by the difference  $(b_o - \frac{a_o}{3})$ ] decreases on heating and vanishes at room temperature, as shown in Fig. 4. Due to its higher symmetry and the better stability of the refinements, we chose to use the structure description with the symmetry of space group  $C222_1$ . It was also applied to the data obtained for the  $x=0.25$  sample. Good quality Rietveld refinements (see Ref. 25) were obtained at temperatures above 240 K ( $\chi^2=4.01$  at 300 K), indicating that the same type of structural distortion is present for this composition. In this sample, the ordering of Rb cations occurs between 200 and 240 K as shown by the appearance of small superstructure peaks similar to those first observed by Sato *et al.*<sup>27</sup> Below 200 K, the agreements become slightly worse ( $\chi^2=6.43$  at 5 K) because the superstructure is not taken into account in this structural model. A summary of the refined parameters and principal interatomic distances are given in Tables I–III for  $T=5$  and 300 K.

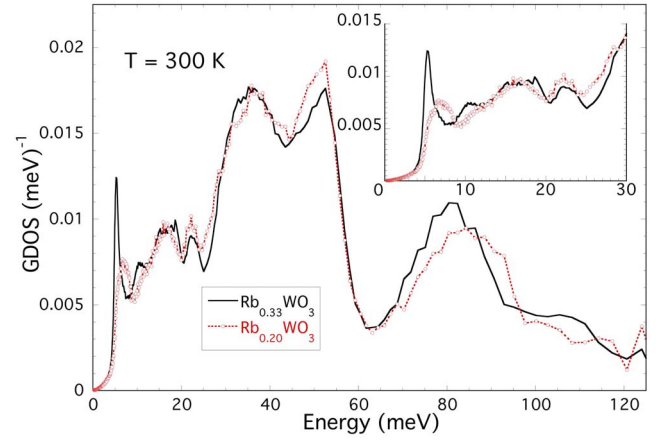


FIG. 5. (Color online) Generalized phonon density of states in  $\text{Rb}_{0.33}\text{WO}_3$  (solid lines) and  $\text{Rb}_{0.20}\text{WO}_3$  [dotted lines and open circles in red color (gray)] deduced from INS experiments at 300 K in the absence of a cryostat. The inset displays a blowup of the low-energy range.

### C. Phonon density of states and generalized phonon density of states

An overall picture of the generalized phonon density of states  $G_e(\omega)$  deduced from our INS experiments is presented in Fig. 5. These data have been obtained on  $\text{Rb}_{0.33}\text{WO}_3$  and  $\text{Rb}_{0.20}\text{WO}_3$  samples which were simply wrapped in an aluminum foil and placed directly in the beam at ambient temperature and atmosphere. Getting rid of the cryostat allows us to reduce the error introduced by subtracting the background scattering.<sup>28</sup> In order to describe and discuss more conveniently the GDOS spectra, we will distinguish therein four main regions covering approximately the following energy ranges: (i) region I between 0 and about 10 meV; (ii) region II between about 10 and 25 meV; (iii) region III between about 25 and 60 meV; (iv) region IV between about 60 and 120 meV.

The more obvious difference between the GDOS observed in the two compounds concerns region I, where the well-defined peak observed in the stoichiometric compound just above 5 meV seems to have collapsed in  $\text{Rb}_{0.20}\text{WO}_3$ . Simultaneously, the first minimum is shifted from  $\sim 7.5$  to  $\sim 9.1$  meV and replaced by a blunt maximum between 6.5 and 7.5 meV. Among the other small differences between the two spectra, we notice the slightly larger GDOS observed in  $\text{Rb}_{0.20}\text{WO}_3$  in the  $\sim 20$ – $27$  and  $\sim 45$ – $55$  meV ranges, as well as a sensible hardening in region IV. Although less accurate, the data obtained with the samples inside the cryostat (Fig. 6) indicate that these Rb-content-related differences seem to develop continuously and does not make  $\text{Rb}_{0.25}\text{WO}_3$  ( $T_c \leq 0.2$  K) significantly different from  $\text{Rb}_{0.20}\text{WO}_3$  ( $T_c \geq 5$  K). From our measurements at  $T=100$  K on the three samples, we have derived the generalized density of states shown in Fig. 7, where they are compared to the room-temperature results obtained under the same experimental conditions. The energy range is restricted here to below  $\approx 3k_B T \approx 30$  meV due to the sharply decreasing thermal occupation of the phonons. In order to check for a possible

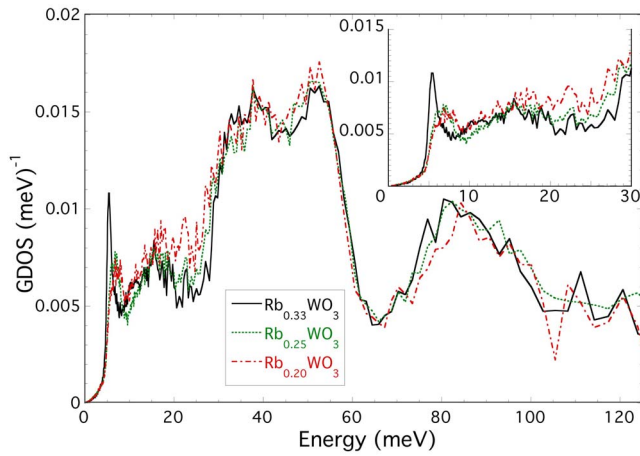


FIG. 6. (Color online) Generalized phonon density of states in  $\text{Rb}_x\text{WO}_3$  deduced from INS experiments at 300 K in the cryostat [ $x=0.33$ , black solid lines;  $x=0.25$ , green (gray) dotted lines; and  $x=0.20$ , red (dark gray) dashed lines]. The inset displays a magnification of the low-energy range.

effect of the Rb ordering in  $\text{Rb}_{0.20}\text{WO}_3$ , we compared the spectral response of the same sample after it has been slowly cooled, on the one hand, and after it has been cooled down to 100 K in about 1 min by immersion in liquid  $\text{N}_2$  and consecutive transfer at this temperature into the cryostat, on the other hand. No difference could be detected between these two experiments, within the data statistics.

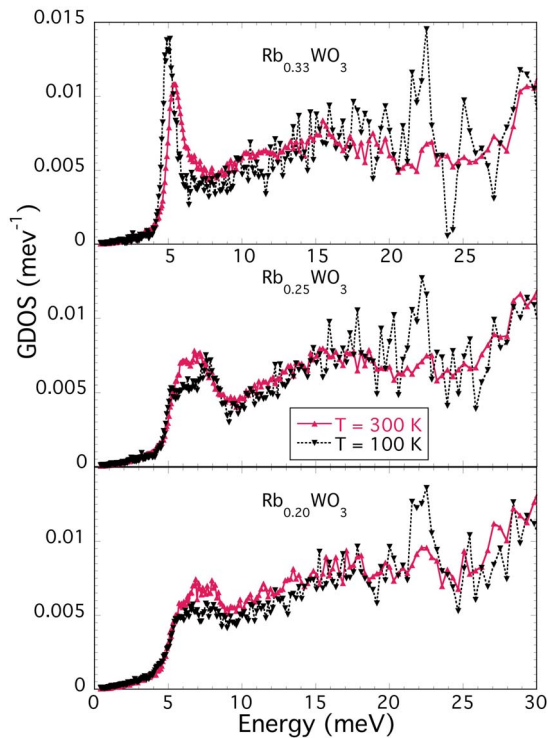


FIG. 7. (Color online) Generalized phonon density of states in  $\text{Rb}_x\text{WO}_3$  at  $T=300$  K [solid lines and  $\blacktriangle$  in red (gray) color] and  $T=100$  K (dotted black lines and  $\blacktriangledown$ ).

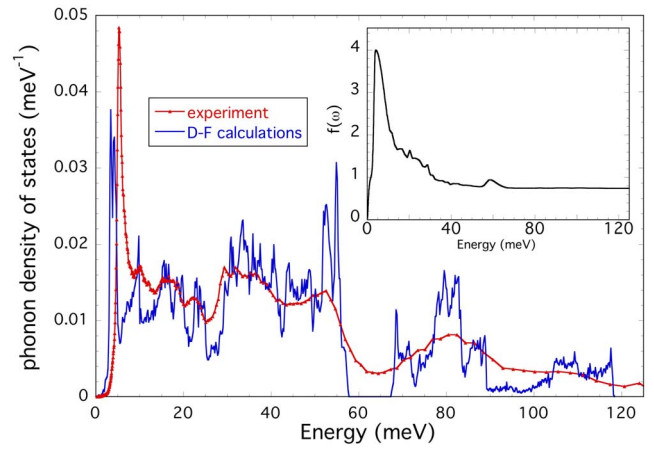


FIG. 8. (Color online) Phonon density of states of  $\text{Rb}_{0.33}\text{WO}_3$ : DFT calculations [blue (dark gray) line] and IN6 experiment at  $T=300$  K [red (gray) line with small markers] deduced from the measured GDOS displayed in Fig. 5. The inset shows the weighting factor relating DOS and GDOS (see Sec. III D).

#### D. Density-functional theory calculations

In Fig. 8, we compare the calculated  $g(\omega)$  for  $\text{Rb}_{0.33}\text{WO}_3$  in  $C222_1$  symmetry with the experimental data. The agreement is very good even down to small details. We, e.g., exactly reproduce the four peaks in  $g(\omega)$  measured between 8 and 25 meV (region II). It is, as already mentioned, not possible to stabilize the structure of  $\text{Rb}_{0.33}\text{WO}_3$  in  $P3$  symmetry. This changes when we go to  $\text{Cs}_{0.33}\text{WO}_3$ . Due to the large size of the Cs ion, the hexagonal  $P6_3/mcm$  is stable, provided we use a supercell of similar size as that employed for the calculations on  $\text{Rb}_{0.33}\text{WO}_3$ . For both compounds and structures, the calculated lattice parameters agree very well with the measured values, as displayed in Table IV. The dynamic response of  $M_{0.33}\text{WO}_3$  ( $M=\text{Rb}$  and  $\text{Cs}$ ) is clearly separated into various vibrational bands. Using the fact that the DFT calculation provides us with the complete set of phonon eigenvectors, we may decompose the density of states into its partial components. A further characterization is obtained by separating the partial DOS into contributions that arise by projecting the eigenvectors either into the basal  $x$ - $y$  plane of the channels or perpendicular to it. In Fig. 9, we show the partial phonon DOS for  $\text{Cs}_{0.33}\text{WO}_3$ . The low-frequency part of the spectrum (region I) is dominated by the motion of the guest ion within the cage. This motion is characterized by a strong anisotropy. The motion within the basal

TABLE IV. Calculated and experimental lattice parameters (from Ref. 29 for the Cs bronze).

Model	$a$ (Å)	$b$ (Å)	$c$ (Å)	$b-a\sqrt{3}$ (Å)
$\text{Cs}_{0.33}\text{WO}_3$	7.480	7.480	7.687	
Experiment	7.4116(3)	7.4116(3)	7.5981(5)	
$\text{Rb}_{0.33}\text{WO}_3$	12.938	7.473	7.660	-0.0059
Experiment	12.751	7.373	7.531	-0.0188

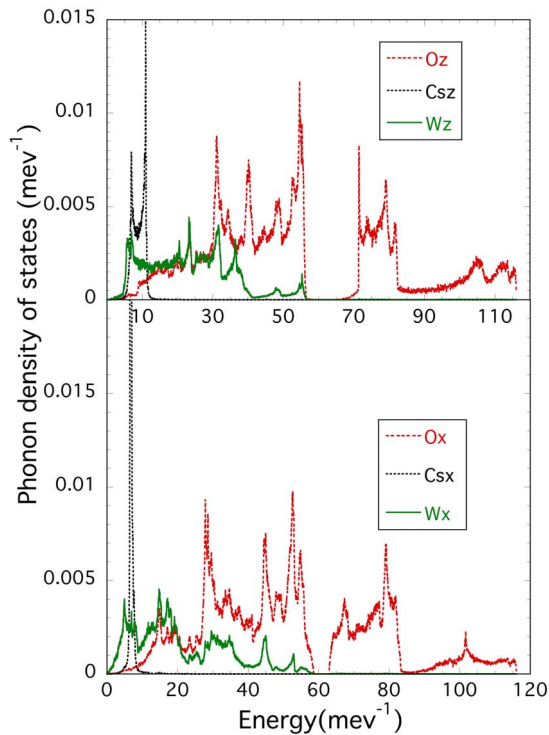


FIG. 9. (Color online) Partial phonon density of states in  $\text{Cs}_{0.33}\text{WO}_3$  separated into contributions arising by projecting the eigenvectors into and perpendicular to the basal  $x$ - $y$  plane of the channels. The  $y$  component is not shown as it is indistinguishable from the  $x$  component. Dashed red (gray) lines correspond to O contributions, dotted black lines to Cs contributions, and solid green (gray) lines to W contributions.

plane has very little dispersion, leading to a sharply peaked and narrow structure at about 6 meV. In  $\text{Rb}_{0.33}\text{WO}_3$ , this in-plane motion is softer. It actually comes out somewhat too low if compared with the experiment. Given the uncertainties in the calculations, this discrepancy should, however, not be overestimated as deviations of a few meV are common for DFT based phonon calculations. The softening of  $\text{Rb}_{0.33}\text{WO}_3$  with respect to  $\text{Cs}_{0.33}\text{WO}_3$  indicates that the size of the  $M$  ions plays a role in the bonding. If this was not the case, then the lighter Rb should vibrate at higher frequencies than Cs. Compared to the in-plane motion, the vibrations of the  $M$  ions along the channel are spread out over a more extended range in energy, giving a band with a tuning fork shape. Inspection of the eigenvectors shows that the two spikes of the fork correspond to in-phase (all ions in a channel move in the same direction) and out-of phase (alternating ions in a channel move in opposite directions) motion of  $M$  ions. For the out-of-phase motion, there is an additional restoring force arising from the Coulomb repulsion between the  $M$  ions, lifting the frequency to beyond 10 meV. For the in-phase motion, the distance between the  $M$  ions does not change and the Coulomb repulsion is inactive. The frequency, thus, drops to frequencies very close to those of the in-plane motions.

The W ions take part in the vibrations up to 60 meV (regions I–III), and there is a marked anisotropy in the vibra-

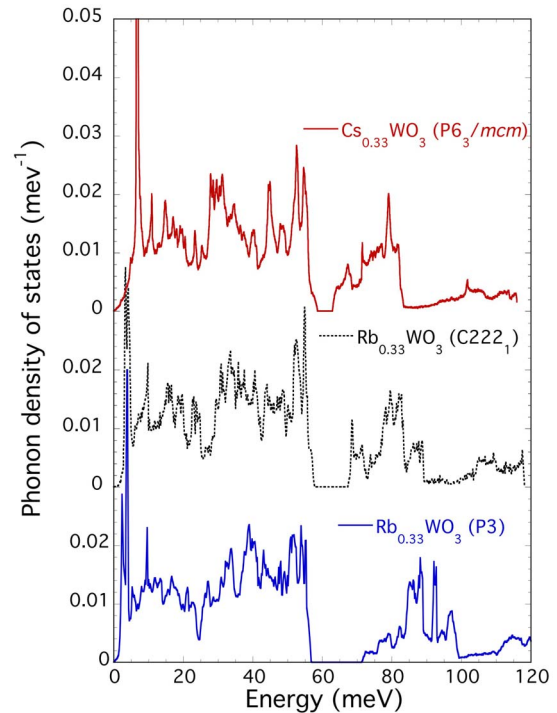


FIG. 10. (Color online) Calculated phonon density of states for two ( $P3$  and  $C222_1$ )  $\text{Rb}_{0.33}\text{WO}_3$  and one  $\text{Cs}_{0.33}\text{WO}_3$  ( $P6_3$ ) structures.

tional frequencies. The low-frequency part of the W partial DOS is softer in  $\text{Cs}_{0.33}\text{WO}_3$  as compared to  $\text{Rb}_{0.33}\text{WO}_3$ . W, in this respect, shows a behavior opposite to that of the  $M$  ion vibrations.

The anisotropy of the crystal structure is equally visible in the oxygen spectra. O vibrations cover the full range from zero to 120 meV. The participation of O in the low-frequency vibrations (region I) is not limited to the acoustic modes. We equally find in this range eigenvectors describing collective rotations of the  $\text{WO}_6$  octahedra. As the frequency increases, there are more and more distorting contributions to these rigid-unit modes. At intermediate frequencies (regions II and III), distortion takes place perpendicular to the strong W-O covalent bond. At the high-frequency end (region IV), the W-O bonds are solicited in W-O stretching modes. The frequency of these stretching modes depends crucially on the W-O bond length distribution. In Fig. 10, we compare the calculated density of states for two ( $P3$  and  $C222_1$ )  $\text{Rb}_{0.33}\text{WO}_3$  and one  $\text{Cs}_{0.33}\text{WO}_3$  ( $P6_3$ ) structures. The fact that the calculations are unable to produce a stable  $\text{Rb}_{0.33}\text{WO}_3$  crystal within the  $P3$  symmetry group and, thus, produce negative values of the dynamical matrix is of no importance for the high-frequency end of the spectrum. We clearly observe important shifts of the oxygen bands, in particular, of the stretching modes in region IV. This is not surprising as the  $\text{WO}_6$  octahedra in  $\text{Rb}_{0.33}\text{WO}_3$  in  $P3$  can be characterized as more distorted, giving, in particular, larger extremes for the smallest and largest W-O distance, respectively. The calculated O spectrum of  $\text{Cs}_{0.33}\text{WO}_3$  ( $P6_3$ ) is, on the contrary, rather close to that in  $\text{Rb}_{0.33}\text{WO}_3$  ( $C222_1$ ).

### Generalized and “true” phonon densities of states

In the preceding section, we have presented a true density of states obtained from the experimental data. We shall concisely establish how we determine the conversion factor  $f(\omega)$  relating the two quantities. In principle, it could be fully calculated from the DFT results. Actually, the acoustic part of the spectrum, below about 4 meV, is not very well described by our density-functional calculations: this is quite a usual shortcoming and results in overestimating the ratio  $f(\omega)$  in this range. This ratio should approach unity as  $\omega$  tends to zero; however, the experimental  $G_e(\omega)$  is also overestimated below about 1.5 meV, due to spurious detection of elastic contributions. Consequently, the ratio—we shall call it  $f_e(\omega)$ —between the true experimental  $g_e(\omega)$  and the measured  $G_e(\omega)$  will decrease below unity as  $\omega$  goes to zero.

A more precise estimate of the low-energy behavior of  $f_e(\omega)$  can be derived from a comparison between the lattice specific heat ( $C_p$ ) obtained from  $g_e(\omega)$  and the direct experimental determinations by Bevolò *et al.*<sup>30</sup> and King *et al.*<sup>31</sup> The main feature of  $C_p$  below  $\sim 40$  K is an excess contribution which can be well fitted to an Einstein mode with a characteristic temperature  $\theta_E \approx 58$  K in  $\text{Rb}_{0.33}\text{WO}_3$ . This mode evidently corresponds to the well-defined peak of  $g(\omega)$  at 5.3 meV. Another piece of information given by the measured  $C_p$  is the Debye temperature  $\theta_D$  King *et al.* estimated from the “normal” part of the specific heat, between 2 and 3 K, i.e.,  $\theta_D = 415 \pm 15$  K: a  $\omega^2$  fit of our  $g_e(\omega)$  below  $\sim 2$  meV should give us a similar value of  $\theta_D$ . Finally, a corrected  $f_e(\omega)$  which satisfies the specific-heat requirements is displayed in the inset of Fig. 8. It yields the experimental  $g_e(\omega) = f_e(\omega)G_e(\omega)$  displayed in the same figure. Our derivation is also confirmed by the number of modes one can count within the 4–9 meV range, and which is now consistent with what is expected from the Rb population (7.7%). It is the preponderance of the Rb modes in this range, which explains the large low-energy maximum in  $f_e(\omega)$ .

## IV. DISCUSSION

### A. Magnetic properties

Let us first review the different contributions entering the measured magnetic susceptibility  $\chi_x$ , considering first the stoichiometric compound  $\text{Rb}_{0.33}\text{WO}_3$ .

The diamagnetic core component  $\chi_{\text{core}}$  is usually identified with the ionic contributions which have been compiled by Klemm:<sup>32</sup> this gives  $-20 \times 10^{-6}$  emu/g ion for  $\text{Rb}^+$ .<sup>33</sup> Similarly, following Klemm would give  $-49 \times 10^{-6}$  emu/mole for the diamagnetic core contribution of  $\text{WO}_3$ ; however this compound is much less diamagnetic due to a significant Van Vleck (VV) paramagnetism,  $\chi_{\text{VV}}$ . As a first approximation, we shall suppose that  $\chi_{\text{core}}$  and  $\chi_{\text{VV}}$  are the same in  $\text{WO}_3$  and in  $\text{Rb}_{0.33}\text{WO}_3$ . Accordingly, we take for the susceptibility  $\chi_{\text{loc}}$  of the localized electrons in  $\text{Rb}_{0.33}\text{WO}_3$ :

$$\chi_{\text{loc}}(\text{Rb}_{0.33}\text{WO}_3) \approx \chi_{\text{core}}(\text{Rb}_{0.33}^+) + \chi(\text{WO}_3).$$

Unfortunately,  $\chi(\text{WO}_3)$  is not known very precisely, and the published values<sup>34</sup> range between  $-13 \times 10^{-6}$  and  $-21 \times 10^{-6}$  emu/mole.<sup>35</sup>

Another paramagnetic contribution is expected from the spin susceptibility of the conduction electrons  $\chi_{\text{spin}}$  (or Pauli susceptibility). As far as  $\text{Rb}_{0.33}\text{WO}_3$  is concerned,  $\chi_{\text{spin}}$  can be roughly determined by using the electronic coefficient of the specific heat  $\gamma$ , which has been estimated between 2.2 mJ/K<sup>2</sup> mole (Ref. 31) and 1.9 mJ/K<sup>2</sup> mole.<sup>30</sup> The corresponding electron density of states at the Fermi level  $D_{\text{FE}}$  would be about  $0.87 \pm 0.07$  state/eV molecule and  $\chi_{\text{spin}} \approx 7.8 \pm 0.6 \times 10^{-7}$  emu or  $28 \pm 2 \times 10^{-6}$  emu/mole. These values are about two times larger than expected from a free-electron band containing  $x$  electron per W atom and it is also what is observed, on average, in the other alkali tungsten bronzes.<sup>36</sup> The composition dependence of  $\chi_x$ , which would result only from the  $x$  dependence of  $\chi_{\text{spin}}$ , is plotted in Fig. 2.

Finally, an orbital contribution of the conduction electrons,  $\chi_L$ , is expected from the Landau mechanism: it partly compensates the Pauli susceptibility when we are dealing with a free electron gas ( $\chi_L = -1/3\chi_{\text{spin}}$ ), but its absolute value is higher the smaller the electron effective mass. Comparing the contributions estimated above to the total measured susceptibility ( $\chi_x = -7.4 \pm 0.3 \times 10^{-6}$  emu/mole for  $\text{Rb}_{0.33}\text{WO}_3$  at 280 K) gives  $\chi_L = \chi_x - (\chi_{\text{loc}} + \chi_{\text{spin}}) = -7.8 \pm 2.3 \times 10^{-6}$  emu/mole, taking  $\chi = -21 \times 10^{-6}$  emu/mole for the susceptibility of  $\text{WO}_3$ .<sup>37</sup> Such a value for  $\chi_L$  seems to confirm the quasi-free-electron-like behavior. This agreement could be somewhat fortuitous, considering our poor knowledge of the other contributions; however, it is supported by the fact that all the investigations carried out on the tungsten bronzes have never revealed a more complex behavior. In particular, we have no experimental or theoretical<sup>38,39</sup> indication that  $D_{\text{FE}}$  could increase noticeably when  $x$  and the electron population decrease.

As an aside, we notice that a similar decomposition should hold for the ITB phases of  $\text{Rb}_x\text{WO}_3$ , therefore a few percent of these phases should not have a sensible effect on the susceptibility of the  $\text{Rb}_{0.20}\text{WO}_3$  sample.

Let us now consider the main problem raised by our data, namely, the effect of the order-disorder transition. The small susceptibility increase at the transition toward the ordered state in  $\text{Rb}_{0.25}\text{WO}_3$  could be attributed to a corresponding increase of the electronic density of states  $D_{\text{FE}}$ , but this would contradict the drastic destabilization of the superconducting state in this compound. Another possibility is that the ordering of the rubidium vacancies simultaneously modifies both  $\chi_{\text{spin}}$  and  $\chi_L$  (and eventually  $\chi_{\text{VV}}$ ): an increase of  $\chi_L$  (and eventually  $\chi_{\text{VV}}$ ) compensating for a decrease of  $D_{\text{FE}}$  and  $\chi_{\text{spin}}$ . This hypothesis seems to be supported by the electronic band structure study of Lee *et al.*,<sup>38</sup> according to which a part of the Fermi surface is quasi-one-dimensional in the disordered state: the superstructure accompanying the ordering could create electron and hole pockets in place of the initial warped sheets, therefore reducing  $D_{\text{FE}}$  and generating possible mechanisms for an increase of  $\chi_L$ . However, in the framework of the BCS model, a reduction of  $D_{\text{FE}}$  by about 40% (Ref. 40) would be necessary to explain, on its own, the corresponding destabilization of the superconducting state. This seems implausible, first, because the main part of the Fermi surface is three-dimensional and should not be perturbed by the ordering. Second, because the ordering only

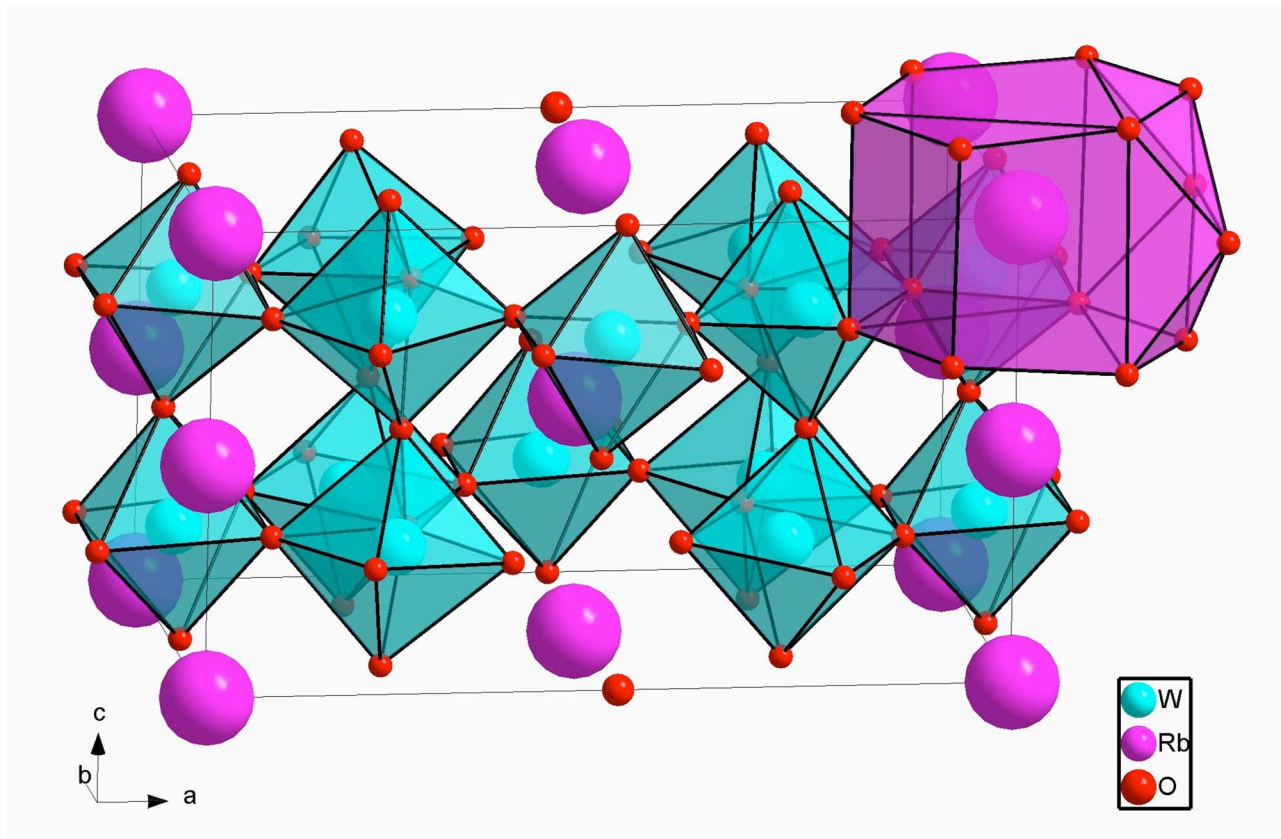


FIG. 11. (Color online) Crystallographic structure of  $\text{Rb}_{0.33}\text{WO}_3$  at 5 K. The smallest red (dark gray) spheres represent the oxygen atoms, the largest fuchsia (gray) spheres represent the rubidium atoms, and the medium-sized turquoise (light gray) spheres represent the tungsten atoms.

concerns a small part of the atoms (1/4 of the Rb atoms are missing in  $\text{Rb}_{0.25}\text{WO}_3$ , i.e., only 2% of the total population).

We are, therefore, prone to conclude that if there is any reduction of  $D_{\text{FE}}$  induced by the ordering, it cannot be large enough to explain the drastic reduction of  $T_c$ , contrary to most of the previous interpretations.

### B. Structural properties

The main result of this structural study is the improvement brought about by adopting a description of slightly lower symmetry than before, the better one compatible with the low-temperature data. Moreover, it appears now that the rubidium bronze is farther from the strict hexagonal symmetry the lower is the temperature. On the contrary, they probably recover the full hexagonal  $P6_3/mcm$  symmetry above room temperature, as we shall discuss below. It is worth emphasizing that our attribution of the  $C222_1$  symmetry to these bronzes has been remarkably confirmed by the density-functional calculations we have performed to describe the lattice dynamics of these compounds (see Sec. III D). Actually, this symmetry allows us to produce not only a completely relaxed structure (no residual forces acting on the atoms) but also an equally stable structure (no negative eigenvalues of the dynamical matrix), whereas the formerly proposed symmetries  $P6_3/mcm$  and  $P3$  lead to an unstable lattice.

By comparing our  $C222_1$  description with the previous ones, we notice a slightly different oxygen environment around the rubidium atoms: instead of 12 nearest neighbors at 3.30 Å plus six second nearest at 3.52 Å corresponding to the  $P6_3/mcm$  configuration, we find the 12 nearest neighbors between 3.26 and 3.36 Å, and two O5 oxygen at 3.434 Å in the stoichiometric bronze at 300 K. This coordination is illustrated in Fig. 11. The large amplitude of the Rb vibrations within this oxygen cage is manifested in the large associated atomic displacement parameter at room temperature:  $B \approx 3.5$  Å. It should be noted that this value is higher than that observed in  $\text{RbOs}_2\text{O}_6$ , where it has attracted considerable attention and has been associated with some rattling mode.<sup>41</sup> Except for the superstructure which accompanies the vacancy ordering in  $\text{Rb}_{0.25}\text{WO}_3$ , no drastic structural changes are observed between this nonsuperconducting compound and the stoichiometric superconducting  $\text{Rb}_{0.33}\text{WO}_3$ . The principal differences are illustrated in Figs. 4 and 12, and can be summarized as follows:

(i) At 300 K, the reduction of the Rb content notably increases the distortion of the  $\text{WO}_6$  octahedra around W1, whereas it slightly reduces the distortion around W2. Therefore, in  $\text{Rb}_{0.25}\text{WO}_3$ , the W1 population is distinguished very clearly from the numerically equivalent W2 population, whereas in  $\text{Rb}_{0.33}\text{WO}_3$ , this distinction is small enough that it could pass unnoticed in the previous works. Although the difference between the two compounds lessens as the tem-

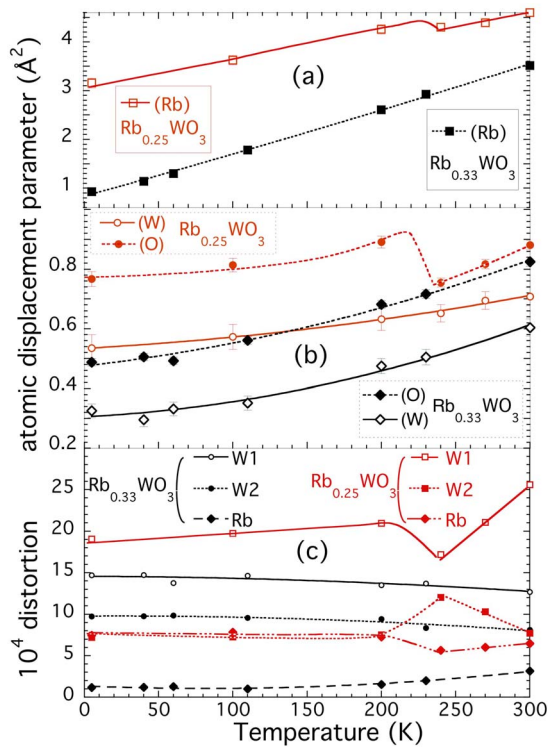


FIG. 12. (Color online) Temperature dependence of the [(a) and (b)] isotropic atomic displacement parameter  $B$  and (c) distortion in  $\text{Rb}_{0.33}\text{WO}_3$  (black lines and markers) and  $\text{Rb}_{0.25}\text{WO}_3$  [red (gray) lines and markers].

perature decreases (cooling reduces the distortion in  $\text{Rb}_{0.25}\text{WO}_3$ , whereas the opposite happens in  $\text{Rb}_{0.33}\text{WO}_3$ ), the distinction between the W1-centered and W2-centered octahedra is still well marked in  $\text{Rb}_{0.25}\text{WO}_3$  at 5 K.

(ii) Lowering the temperature has an opposite effect on the oxygen cage surrounding the rubidium, which leads, at 5 K, to quite a spherical cage in  $\text{Rb}_{0.33}\text{WO}_3$ , but to a much more distorted one in  $\text{Rb}_{0.25}\text{WO}_3$ .

(iii) The small distortion associated with the  $(b_o - \frac{a_o}{\sqrt{3}})$  difference is more stable in  $\text{Rb}_{0.25}\text{WO}_3$  than in  $\text{Rb}_{0.33}\text{WO}_3$ : more precisely, the differences plotted in Fig. 4 vanish at 375 and 295 K, respectively, when extrapolated with a second-order polynomial. This is clearly reminiscent of the structural phase transition observed by Sato *et al.*, although the transition temperatures  $T_{c1}$  above which they found the rubidium tungsten bronzes recover the  $P6_3/mcm$  symmetry are markedly higher ( $420 \text{ K} \leq T_{c1} \leq 450 \text{ K}$ ).

(iv) The ordering of the Rb vacancies in  $\text{Rb}_{0.25}\text{WO}_3$  clearly appears through an increase of the atomic displacement parameter  $B$  of the rubidium, but also of the oxygen atoms. This ordering is also manifested in an opposite effect on the distortion of the oxygen cage around W1 and W2, whereas it increases the distortion around Rb (Fig. 12).

### C. Lattice dynamics and phonon density of states

As discussed in Sec. III D, the DOS  $g_c(\omega)$  deduced from our density-functional calculations on  $\text{Rb}_{0.33}\text{WO}_3$  compares

remarkably well with our measurements and allows us to characterize precisely the four energy ranges distinguished above: (i) The Rb vibrations only contribute to region I; (ii) the W vibrations are spread within the second half of region I, and the whole regions II and III, with a maximum contribution between about 7 and 25 meV; and (iii) the oxygen vibrations contribute to the whole spectrum but dominate region III, and take up alone the highest-energy region IV, in which the oxygen vibrations are directed toward the tungsten atoms. An energy gap, centered around 60 meV, separates these modes from the softer ones for which the oxygen vibrations are not directed toward the tungsten atoms. Our calculations also bring to the fore that the oxygen contribution largely dominates the GDOS (94%), whereas the Rb and W atoms participate for only about 3% each, due to their much lower  $\sigma_i/m_i$  coefficients. Consequently, as the tungsten modes are spread in a rather large energy range they share with oxygen modes, they are completely masked by the latter. The Rb modes are fortunately more visible because they are concentrated at lower energies in a narrower range. More precisely, the peak at about 5 meV in  $\text{Rb}_{0.33}\text{WO}_3$  is to be attributed to the motion of the Rb ions in the  $x$ - $y$  i.e., equatorial plane of the cavities these ions fill within the  $\text{WO}_3$  skeleton. The vibrations along the channels which link these cavities along the  $c$  axis are spread between  $\sim 5$  meV, corresponding to in-phase motion of the alkali ions, and  $\sim 10$  meV, corresponding to their out-of-phase motion, in an energy band with a tuning fork shape. The highest-energy spike of this fork coincide with the shoulder observed in  $G_c(\omega)$  at  $\sim 10$  meV.

#### 1. Dependence of the phonon density of states spectrum on the rubidium content

Let us now consider how these features evolve when the Rb population decreases, leaving vacant sites in the tunnels. As we noticed in Sec. III C, the sharp peak at  $\sim 5$  meV broadens and shifts to higher energies; concomitantly, the hump at  $\sim 10$  meV disappears. This is illustrated in Figs. 5 and 6. The broadening is clearly related to the disorder within the Rb sublattice and to the corresponding distribution of local environments seen by the Rb ions. A part of the equatorial band is simultaneously shifted to higher energies, which probably results from the following mechanism: the Rb ions which have lost one of their neighbors should tend to get closer to these vacancies, and the  $\text{WO}_3$  matrix to readjust around them—reacting both to the missing charge transfer and to the shifts of the remaining Rb ions. In this defective environment, the Rb ions are a little more tightly bound in the equatorial plane and the corresponding vibrations are slightly stiffer.

On the contrary, the out-of-phase motion of these ions toward the neighboring vacancy, i.e., along the channels, is easier and the corresponding vibrations are softer. Since increasing the vacancy content also reduces the difference between the in-phase and out-of-phase motions along the  $c$  axis, its global effect on the phonon DOS in region I is to attenuate the well-defined structures observed in the absence of vacancies—the sharp peak at  $\sim 5$  meV and the shoulder at

$\sim 10$  meV—and to fill in the formerly low-density-of-states region in between.

In regions II and III of the phonon DOS spectra, the changes induced by an increasing deviation from stoichiometry are not very pronounced and not easy to interpret since many different modes are involved here and nonstoichiometry cannot be taken into account by our calculations. However, in region IV, the clear hardening, which is observed on the rising edge of the band (by  $\sim 5$  meV) when up to one-third of the Rb ions is removed, can be explained by the shortening of the mean W-O distance.

## 2. Dependence of the phonon density of states on temperature

Within the limited energy range accessible experimentally, the more important modifications induced by lowering the temperature are observed between 4 and 9 meV, where the Rb modes are predominant (see Fig. 7). The most impressive effect is the softening and concomitant narrowing of the band of equatorial Rb vibrations at  $\sim 5$  meV in  $\text{Rb}_{0.33}\text{WO}_3$ . Usually, the anharmonic terms that enter the atomic potentials render them softer at larger displacements. This is why, in general, the restoring forces an ion experiences become stronger as the mean square displacement decreases with temperature, leading to higher frequencies. A particularly strong hardening of this type is, e.g., observed for the  $C_{60}$  librations in superconducting  $\text{Rb}_3C_{60}$ .<sup>42</sup> It is not associated with a broadening of the band. Softening is possible if the potential has a troughlike character or if, in the extreme case, the particle is confined geometrically in a stiff environment described theoretically by a potential well. Such phenomena are observed in many guest-host systems, where a small molecule is loosely bound in a cage. An instructive example is  $\text{N}_2$  hydrate clathrate.<sup>43</sup> While the  $\text{N}_2$  molecules are vibrating against the cage walls at elevated temperatures, they perform a tumbling motion in a troughlike potential at low temperatures. However, in such a case, the softening is accompanied by pronounced damping. A very narrow band in  $\text{Rb}_{0.33}\text{WO}_3$  at 100 K indicates that the Rb ions experience both a harmonic and homogeneous environment—a fact which already emerged from our Rietveld analysis of the structure (see Sec. IV B and Fig. 12). In addition, a narrow band does not allow for band dispersion. Therefore, at 100 K, the Rb ions vibrate in the equatorial plane harmonically and decoupled from each other like perfect Einstein oscillators. The softening is, therefore, to be explained purely by the evolution of the Rb ion environment, leading to a fine tuning of the force constants. It is interesting to note that the DFT calculations produce always a tiny splitting within the narrow Rb band (see Figs. 8 and 13), which even if real would be difficult to observe in the experimental spectra. No softening of the equatorial Rb band is observed in the nonstoichiometric compounds. However, in  $\text{Rb}_{0.25}\text{WO}_3$ , cooling seems to promote a second peak at  $\sim 7.6$  meV, in agreement with what Sato *et al.* observed on a sample of approximate composition  $\text{Rb}_{0.27}\text{WO}_3$ . As this effect is not found in  $\text{Rb}_{0.20}\text{WO}_3$ , it is tempting to relate it to the ordering of the Rb vacancies, which is optimal when 1/4 of the alkali are missing. In the case of  $\text{Rb}_{0.20}\text{WO}_3$ , the only clear sign of anharmonicity is a small low-frequency shoulder that appears in the 100 K

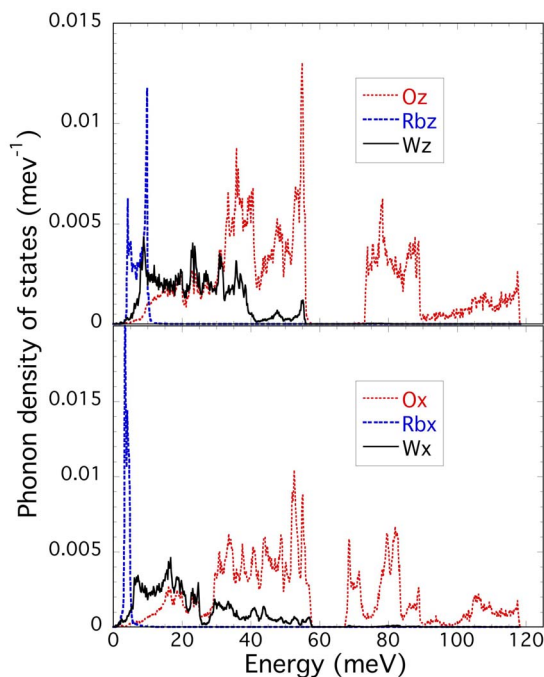


FIG. 13. (Color online) Partial phonon density of states in  $\text{Rb}_{0.33}\text{WO}_3$  separated into contributions arising by projecting the eigenvectors into and perpendicular to the basal  $x$ - $y$  plane of the channels. The  $y$  component is not shown as it is indistinguishable from the  $x$  component. Dashed red (light gray) lines correspond to O contributions, dotted blue (gray) lines to Rb contributions, and solid black lines to W contributions.

spectrum at about 4 meV. This is also the only feature that could recall a contribution from local structural excitations and the LSE model proposed by Ngai and Silbergliitt.<sup>44</sup> This clue seems too tenuous—confronted with the “ $T_c$  ( $x$ ) paradox”—to support this model.

## V. GENERAL DISCUSSION

If we consider the totality of our results, then it turns out that what favors or destabilizes superconductivity in the  $\text{Rb}_x\text{WO}_3$  system is much more subtle than thought up to now. First, we have shown in Sec. IV A that there is no sign of a sensible increase of the electronic density of states  $D_{\text{FE}}$  near  $x=0.20$ , the low-rubidium-content boundary where the highest  $T_c$  is observed, nor is there a significant decrease of  $D_{\text{FE}}$  induced by the ordering of the Rb vacancies, which destroys superconductivity in  $\text{Rb}_x\text{WO}_3$ ; quite to the contrary, this ordering may even lead to a slight increase in  $D_{\text{FE}}$ .

Second, the crystallographic structure of this compound displays only minor differences if compared to that of the stoichiometric  $\text{Rb}_{0.33}\text{WO}_3$ . They can principally be summarized as a slightly more marked difference between the oxygen octahedra surrounding the W1 and W2 sites, respectively. Unfortunately, we have not been able to extend this comparison up to  $\text{Rb}_{0.20}\text{WO}_3$  but, even if this difference should keep growing, we notice that it does not seem to affect  $D_{\text{FE}}$ .

Third, reducing the rubidium content does not yield a global softening of the lattice; on the contrary, it leads to a loss of low-energy Rb  $x$ -y modes, which are redistributed at higher energy. Moreover, even the high-energy O vibrations in region IV are shifted to higher energy. No sign of softening distinguishes  $\text{Rb}_x\text{WO}_3$  from its nonsuperconducting neighbor. This lack of softening does not contradict the fact that, below this Rb content, the HTB phase is no longer stable. Actually, it is replaced by a mixture with the ITB (pseudo)phases, which themselves consist of mutually intercalating  $\text{WO}_3$  and HTB slabs.

Therefore, it seems that what drives superconductivity in this system must be traced back to a very specific electron-phonon (e-p) interaction, involving closely defined electron states and phonons. This is quite a common issue which pertains to the field of the strong-coupling theory. The Ba, K-bismuthates, the  $M_3\text{C}_{60}$  fullerides, and  $\text{MgB}_2$  are among the systems in which this question has been thoroughly investigated, experimentally and theoretically, without always receiving definitive answers. At present, our case is much less documented and we have to rely on our own results for interpretation.

We shall note first that we cannot discard the possibility that the low-energy phonon band associated with the alkali  $x$ -y vibrations contributes to a significant electron-phonon coupling in the *stoichiometric* HTB. This was initially proposed by Kamitakahara *et al.*,<sup>45</sup> considering some correlation between  $T_c$  and the energy of the Einstein-like peak deduced from the specific-heat excess it generates. Our density-functional calculations *a priori* support this correlation since they find that this peak is shifted up by about 2 meV when substituting Cs for Rb in  $M_{0.33}\text{WO}_3$ , compatible with the lower  $T_c$  of the Cs bronze (about 1 K). If we consider only the mass  $m_A$  of the alkali ions, then their frequencies should scale with  $1/\sqrt{m_A}$ . It is, however, known that in guest-host systems, the size of the guest atom can play a decisive role in determining physical quantities. We should not forget that this size effect stabilizes the hexagonal structure against distortion. The DFT calculations confirm this stabilizing effect and give a slightly stronger restoring force for Cs if compared to Rb. The lattice stabilizing effect has already been discussed by Lee *et al.*<sup>38</sup>

It has been argued against a strong electron-phonon coupling of the alkali modes that the alkali ions were too far from the  $t_{2g}$  orbitals involved at the Fermi level and which emerge from the W  $5d$ -O  $2p$  interaction. However, we have seen that the oxygen displacement parameter  $B$  and the distortion of the  $\text{WO}_6$  octahedra are quite sensitive to the vacancy content and to their ordering (cf. Fig. 12). The magnetic susceptibility and, therefore, the conduction band are also affected by this ordering. To a lesser extent, the neighboring  $\text{WO}_6$  octahedra probably feel the alkali vibrations, and this may influence the conduction band by modulating the W  $5d$ -O  $2p$  hybridizations. The softening of the Einstein-like vibrations at low temperature (cf. Fig. 7) could be a symptom of this contribution to the electron-phonon coupling.

A similar contribution to the electron-phonon coupling has been put forward in the  $\beta$ -pyrochlore osmates  $\text{AOs}_2\text{O}_6$ , in which the large-amplitude motion of the alkali-metal ions

A has been considered to deserve a new qualifier and to be responsible for the superconductivity of these compounds.<sup>46</sup> This may be in the osmates; however, we observe in the tungsten bronzes that reducing the alkali content  $x$  causes the associated Einstein-like peak to collapse. Nevertheless,  $T_c$  increases unless ordering takes place. This means that, even if we accept that the Rb vibrations play a role in the superconductivity, they cannot be made responsible for it on their own. Another part of the phonon spectrum has to be involved in the electron-phonon coupling. However, no clear indication of this mechanism appears in the phonon DOS at 300 K or below 30 meV at 100 K. Two possibilities seem to be left: first, the enhancement of the e-p coupling with decreasing  $x$  concerns such a restricted energy range that it cannot be resolved in our experiment; second, the softening it induces at low temperature occurs above 30 meV—an energy range to which the technique we used gives no access. Such a situation is reminiscent of the significant softening of the oxygen “bond stretching” modes observed in  $\text{Ba}_{0.6}\text{K}_{0.4}\text{BiO}_3$  around 30 and 60 meV.<sup>3,4</sup> It is tempting to suppose a similar process in  $M_x\text{WO}_3$ , where we have the following indications that the e-p coupling could involve high-energy oxygen modes: (i) Walkingshaw *et al.*<sup>47</sup> performed a density-functional study of charge doping in  $\text{WO}_3$ , considering only the effect of the addition of electronic charge (without the inclusion of  $M$  ions and the associated size effects). They showed that reducing the doping level leads to rotations of the  $\text{WO}_6$  octahedra and displacement of the W ion from the center of its octahedron. (ii) It also emerges from our calculations (see Sec. III D) that the energy of an oxygen stretching or breathing mode, above the 60 meV gap, is quite sensitive to the W-O distance involved—which appears when the  $C222_1$  structure of  $\text{Rb}_{0.33}\text{WO}_3$  is replaced by the previously considered  $P3$  symmetry, or when Rb is replaced by Cs ( $P6_3/mcm$  symmetry). (iii) We observed such a sensitivity of vibrations to the W-O distance in  $\text{Rb}_x\text{WO}_3$  at 300 K, near 80 meV (Fig. 6).

Further experiments should be undertaken at low temperature to extend the investigation of the phonon DOS to the region beyond 30 meV. They could be guided by the following remarks: the  $T_c$  increase with decreasing  $x$  would be similar in  $\text{Cs}_x\text{WO}_3$  and  $\text{Rb}_x\text{WO}_3$  if ordering could be prevented in the latter. This could indicate that similar parts of the phonon spectra are involved, despite the somewhat different lattice structure. According to our density-functional calculations, fair coincidences between these spectra occur between 75 and 85 meV for the oxygen (bond stretching) vibrations, and also between 40 and 57 meV (bond bending vibrations), as it appears in Fig. 13. Other coincidences have to be noticed between 30 and 35 meV for the W  $x$ -y vibrations, and between 30 and 56 meV for the  $W_z$  vibrations.

One last question must be considered again, i.e., the detrimental effect of the Rb-vacancy ordering on the stability of the superconducting state. Although this ordering does not lead to a significant depression of  $D_{\text{FE}}$ , it becomes manifest in the magnetic susceptibility (Fig. 1), in the tungsten environment, and in the oxygen displacement parameter (Fig. 12). It therefore generates some alterations in the conduction band. Moreover, it could partly remove (condense) the

phonons engaged in a strong e-p coupling, as suggested by Lee *et al.*,<sup>38</sup> and reduce drastically this coupling via a perhaps fortuitous cooperation of these two mechanisms.

## VI. CONCLUSION

The data we have presented allow us to address in more realistic terms the questions raised by superconductivity in  $\text{Rb}_x\text{WO}_3$  and, more generally, in the hexagonal tungsten bronzes. Our magnetic susceptibility measurements confirm that the increase of  $T_c$  with the Rb impoverishment is not due to an increase in electronic density of states  $D_{FE}$ . They contradict the previously admitted postulate according to which the drastic decrease of  $T_c$  accompanying the Rb ordering results from a deep reduction of  $D_{FE}$ . Our structural study has led us to abandon the previous hexagonal description for the lower symmetry  $C222_1$ . Incidentally, these results emphasize, in agreement with the density-functional calculations,<sup>47</sup> how much the precise arrangement of the  $\text{WO}_6$  octahedra within the  $\text{WO}_3$  skeleton is sensitive to the concentration of conduction electrons brought about by the alkali ions. The oxygen cage surrounding a Rb ion is rather large and allows large amplitude displacements, as noticed in the previous studies. This leads to Rb vibrations which are well decoupled from the rest of the lattice and, particularly, to well-defined Einstein-like modes in the equatorial  $x$ - $y$  plane—at least when all the Rb ions are present because these features rapidly attenuate when the vacancy content increases. The phonon spectra derived from our INS experiments extend up to a rather high energy (120 meV), due to the rigidity of the  $\text{WO}_6$  octahedra, in comparison to which the  $\text{BiO}_6$  octahedra of BKBO look quite soft. The lattice stability and dynamics of the stoichiometric bronzes are very well described by our density-functional calculations, which are able to confirm that the stability of  $\text{Rb}_{0.33}\text{WO}_3$  is ensured by the  $C222_1$  structure and not by the hexagonal symmetry, whereas the stability of  $\text{Cs}_{0.33}\text{WO}_3$  is compatible with the more symmetric  $P6_3/mcm$  structure.

Our INS data also indicate that decreasing the alkali content does not soften the structure at room temperature, and that softening could also be ruled out at low temperature, below 30 meV, except for the Rb  $x$ - $y$  vibrations in the stoichiometric compound. We are tempted to conjecture that a reason why underdoping favors superconductivity could lie in the fact that it slightly remodels the  $\text{WO}_6$  octahedra and makes some associated phonons more active in the e-p coupling. Such phonons are to be searched for above 30 meV, i.e., in a rather unusual energy range, but which yields strong contributions to the e-p coupling in BKBO,  $\text{MgB}_2$ , and the fullerides, for instance. The lower  $T_c$  obtained in the tungsten bronzes, compared to the above materials, could partly result from the particular stiffness of the  $\text{WO}_6$  octahedra, the building blocks of these bronzes. Conversely, the stabilization of the superconducting state at higher temperatures, which has been observed in some marginal situations<sup>48</sup> could have something to do with exotic rotations of the  $\text{WO}_6$  octahedra at the surface or interface, due to reduced atomic coordination. In order to get more insight on the  $T_c(x)$  paradox, we need to complete our INS experiments at lower temperature and higher energy. Refining the lattice structure near the  $x=0.20$  limit could also be fruitful as well as extending similar investigations to the order-free and more symmetrical  $\text{Cs}_x\text{WO}_3$ . This could also help us to understand why superconductivity is destroyed by the slight modulation produced here by the alkali ordering: a phenomenon for which the HTB offer the unique illustration, and which deserves particular theoretical efforts since it has all the potential to tell us something fundamental about the superconducting state.

## ACKNOWLEDGMENTS

The authors would like to thank Jacques Marcus for his help in the preparation of the samples, André Sulpice for his contribution to the magnetic susceptibility measurements, Emanuelle Suard for assistance with experiment on the D2B diffractometer, and Mark Johnson for his invaluable help with the computer codes.

\*rene.brusetti@grenoble.cnrs.fr

<sup>1</sup>A. R. Sweedler, C. J. Raub, and B. T. Matthias, *Phys. Lett.* **15**, 108 (1965).

<sup>2</sup>A. I. Liechtenstein, I. I. Mazin, C. O. Rodriguez, O. Jepsen, O. K. Andersen, and M. Methfessel, *Phys. Rev. B* **44**, 5388 (1991).

<sup>3</sup>C.-K. Loong, P. Vashishta, R. K. Kalia, W. Jin, M. H. Degani, D. G. Hinks, D. L. Price, J. D. Jorgensen, B. Dabrowski, A. W. Mitchell, D. R. Richards, and Y. Zheng, *Phys. Rev. B* **45**, 8052 (1992).

<sup>4</sup>M. Braden, W. Reinhardt, S. Shiryayev, and S. N. Barilo, *Physica C* **378-381**, 89 (2002).

<sup>5</sup>L. A. Klinkova, M. Uchida, Y. Matsui, V. I. Nikolaichik, and N. V. Barkovskii, *Phys. Rev. B* **67**, 140501(R) (2003).

<sup>6</sup>For a review, see, for instance, J. D. Jorgensen, *Phys. Today* **44**(6), 34 (1991).

<sup>7</sup>R. Bruseti, P. Bordet, and J. Marcus, *J. Solid State Chem.* **172**, 148 (2003).

<sup>8</sup>R. Bruseti, P. Haen, and J. Marcus, *Phys. Rev. B* **65**, 144528 (2002).

<sup>9</sup>Unless otherwise specified, the composition of our samples we shall refer to is always the nominal composition. The uncertainty about the actual composition is discussed in Ref. 7.

<sup>10</sup>A. Hussain, *Acta Chem. Scand., Ser. A* **32**, 479 (1978).

<sup>11</sup>As discussed in Ref. 7, the low- $x$  boundary of the HTB phase is not known precisely, and its equilibrium value seems to depend on temperature. Moreover, it is quite difficult to realize equilibrium conditions throughout the cooling down from 900 to 300 K since we are dealing with powder samples under very low pressure. This problem has been probably amplified in the present circumstances, as we have prepared, in a single batch, a much larger amount (15 g) of powder than usual, in order to carry out our neutron scattering experiments.

<sup>12</sup>Such an orientation could also result only from the shape of the microcrystals (due to the demagnetizing effect), but even a very

- small anisotropy of the susceptibility has a much greater orientation effect.
- <sup>13</sup>W. C. Lee and D. C. Johnston, *Phys. Rev. B* **41**, 1904 (1990).
- <sup>14</sup>T. Roisnel and J. Rodríguez-Carvajal, *Materials Science Forum, Proceedings of the European Powder Diffraction Conference (EPDIC7)*, 2001 (unpublished), Vols. 378–381, pp. 118–123.
- <sup>15</sup>K. Parlinski, PHONON software (Cracow, 2003), <http://wolf.ifj.edu.pl/phonon/>
- <sup>16</sup>P. E. Blöchl, *Phys. Rev. B* **50**, 17953 (1994).
- <sup>17</sup>G. Kresse and D. Joubert, *Phys. Rev. B* **59**, 1758 (1999).
- <sup>18</sup>G. Kresse and J. Hafner, *Phys. Rev. B* **47**, 558 (1993); **49**, 14251 (1994).
- <sup>19</sup>G. Kresse and J. Furthmüller, *VASP (Vienna, 1999)*; *Phys. Rev. B* **54**, 11169 (1996); *Comput. Mater. Sci.* **6**, 15 (1996).
- <sup>20</sup>Our magnetization measurements as a function of temperature have been carried under a 2 T magnetic field.
- <sup>21</sup>We notice that this procedure supposes that the intrinsic susceptibility of the bronzes does not depend on temperature (for  $T \leq 120$  K), which is not strictly the case since we still observe a small but systematic temperature dependence after removing the Curie-Weiss terms from our data (see Fig. 1).
- <sup>22</sup>Our use of the Curie-Weiss expression does not imply that we believe that these impurities can directly magnetically interact, but they could interact via the conduction electrons, obeying a kind of Kondo mechanism.
- <sup>23</sup>D. R. Wanlass and M. J. Sienko, *J. Solid State Chem.* **12**, 362 (1975).
- <sup>24</sup>According to M. J. Sienko and S. M. Morehouse, *Inorg. Chem.* **2**, 485 (1963), the accuracy of their susceptibility measurements is about 5%, corresponding to  $2.5 \times 10^{-6}$  emu/g.
- <sup>25</sup>See EPAPS Document No. E-PRBMDO-76-107737 for the Rietveld fits on  $\text{Rb}_{0.33}\text{WO}_3$  and  $\text{Rb}_{0.25}\text{WO}_3$  between 5 and 300 K. For more information on EPAPS, see <http://www.aip.org/pubservs/epaps.html>.
- <sup>26</sup>I. D. Brown and D. Alterman, *Acta Crystallogr., Sect. B: Struct. Sci.* **41**, B244 (1985).
- <sup>27</sup>M. Sato, B. H. Grier, G. Shirane, and H. Fujishita, *Phys. Rev. B* **25**, 501 (1982); M. Sato, B. H. Grier, H. Fujishita, S. Hoshino, and A. R. Moodenbaugh, *J. Phys. C* **16**, 5217 (1983).
- <sup>28</sup>All the GDOS data we presented have been normalized to have  $\int_0^{120 \text{ meV}} G_e(\omega) d\omega = 1$ .
- <sup>29</sup>L. Kihlborg and A. Hussain, *Mater. Res. Bull.* **14**, 677 (1979).
- <sup>30</sup>A. J. Bevolto, H. R. Shanks, P. H. Sildes, and G. C. Danielson, *Phys. Rev. B* **9**, 3220 (1974).
- <sup>31</sup>C. N. King, J. A. Benda, R. L. Greene, and T. H. Geballe, in *Proceedings of the 13th International Conference on Low Temperature Physics, Boulder, CO, 1972*, edited by R. H. Kropschot and K. D. Timmerhaus (University of Colorado Press, Boulder, CO, 1973).
- <sup>32</sup>W. Klemm, in *Zahlenwerte und Funktionen aus Physik, Chemie, Astronomie, Geophysik und Technik.-Bd. 1: Atom- und Molekularphysik.-ITeil: Atom und Ionen*, edited by A. Eucken and K. H. Hellwege (Springer-Verlag, Berlin, 1950), p. 396; quoted by R. R. Gupta [Landolt-Börnstein, New Series, Group II, Vol. 16 (Springer-Verlag, Berlin, 1986), p. 402] and by L. N. Mulay and E. A. Bourdeaux [*Theory and Applications of Molecular Diamagnetism* (Wiley, New York, 1976), p. 306].
- <sup>33</sup>According to Y. G. Dorfman [in *Diamagnetism and the Chemical Bond*, edited by Edward Arnold (Arnold, London, 1965)], this value could include a purely diamagnetic contribution amounting to  $26 \times 10^{-6}$  emu/g ion, plus a Van Vleck contribution corresponding to about  $6 \times 10^{-6}$  emu/g ion.
- <sup>34</sup>See Sienko and Morehouse (Ref. 24). We also measured  $\chi \approx -13 \times 10^{-6}$  emu/mole on a sample of the same Alfa Aesar batch we used to prepare our bronzes.
- <sup>35</sup>Therefore,  $\chi_{VV}$  should amount to  $28 \times 10^{-6}$  emu/mole at the minimum. Similar values have been derived in  $\text{K}_2\text{WO}_4$  and  $\text{Na}_2\text{WO}_4$  ( $27 \times 10^{-6}$  and  $26 \times 10^{-6}$  emu/mole respectively). According to Baudet, such rather large Van Vleck contributions are typical of transition elements in which the  $d$  shell of the valence state is either empty or full [J. Baudet, *J. Chim. Phys. Phys.-Chim. Biol.* **58**, 845 (1961)]. It could also be easily responsible for the small anisotropy which drives the orientation of the microcrystals in a 15 T field.
- <sup>36</sup>M. J. Sienko and B. Banerjee, *J. Am. Chem. Soc.* **83**, 4149 (1961); M. J. Sienko, *Adv. Chem. Ser.* **39**, 224 (1963).
- <sup>37</sup>This seems to be the better choice, corresponding to a highly purified material, although the  $\text{WO}_3$  we used was perhaps not so pure, because we have subtracted the contributions from magnetic impurities to derive  $\chi_x$  from the measured susceptibility.
- <sup>38</sup>K.-S. Lee, D.-K. Seo, and M.-H. Whangbo, *J. Am. Chem. Soc.* **119**, 4043 (1997).
- <sup>39</sup>A. Hjelm, C. G. Granqvist, and J. M. Wills, *Phys. Rev. B* **54**, 2436 (1996).
- <sup>40</sup>For the application of this model to the HTB bronzes, see J. Ranninger and K. P. Sinha, *Proc.-Indian Acad. Sci., Chem. Sci.* **95**, 93 (1985).
- <sup>41</sup>Z. Hiroi, S. Yonezawa, T. Muramatsu, J.-I. Yamaura, and Y. Muraoka, *J. Phys. Soc. Jpn.* **74**, 1255 (2005).
- <sup>42</sup>H. Schober, B. Renker, and F. Gompf, *Physica B* **219-220**, 151 (1996).
- <sup>43</sup>H. Schober, H. Itoh, A. Klapproth, V. Chihaiia, and W. F. Kuhs, *Eur. Phys. J. E* **12**, 41 (2003).
- <sup>44</sup>K. L. Ngai and R. Silbergliitt, *Phys. Rev. B* **13**, 1032 (1976).
- <sup>45</sup>W. A. Kamitakahara, K. Scharnberg, and H. R. Shanks, *Phys. Rev. Lett.* **43**, 1607 (1979).
- <sup>46</sup>M. Brühwiler, S. M. Kazakov, J. Karpinski, and B. Batlogg, *Phys. Rev. B* **73**, 094518 (2006).
- <sup>47</sup>A. D. Walkingshaw, N. A. Spaldin, and E. Artacho, *Phys. Rev. B* **70**, 165110 (2004).
- <sup>48</sup>Extrinsic (probably interfacial) superconductivity has been observed in  $\text{Rb}_x\text{WO}_3$  at  $\sim 8$  K (Ref. 8), and the nucleation of high- $T_c$  superconducting regions on the surface of Na-doped  $\text{WO}_3$  has been claimed by Y. Levi, O. Millo, A. Sharoni, Y. Tsabba, G. Leituss, and S. Reich, *Europhys. Lett.* **51**, 564 (2000).